ACDIV-2018-11
April 2018

Removal of RF-Fingers at the Edges of the Injection Kickers

T. F. Günzel, N. Ayala, F. Fernandez, U. Iriso, M. Pont

Abstract

The ALBA storage ring injection kickers are equipped with RF-fingers to close a 2.5 mm gap between the ceramic tube and the metallic flange. After two distortion incidents that required the replacement of the fingers, their removal was decided. The decision could be supported by the observation that most of the additional impedance is created above the cut-off frequency of the beam pipe. This was later confirmed by a temperature decrease in that zone after the removal. Furthermore it was checked that the thresholds of the longitudinal coupled bunch instabilities of modes trapped around the resulting open gap are above the maximal applied beam current of 400 mA.

Accelerator Division
Alba Synchrotron Light Source
c/ de la Llum, 2-26
08290 Cerdanyola del Valles, Spain

ISBN: 978-3-95450-184-7 doi:10.18429/JACoW-IPAC2018-TUPMK001

REMOVAL OF RF-FINGERS AT THE EDGES OF THE INJECTION KICKERS

T. F. Günzel*, N. Ayala, F. Fernandez, U. Iriso, M. Pont,
ALBA-CELLS Synchrotron, Cerdanyola del Vallès, Spain

Abstract

The ALBA storage ring injection kickers are equipped with RF-fingers to close a 2.5 mm gap between the ceramic tube and the metallic flange. After two distortion incidents that required the replacement of the fingers, their removal was decided. The decision could be supported by the observation that most of the additional impedance is created above the cut-off frequency of the beam pipe. This was later confirmed by a temperature decrease in that zone after the removal. Furthermore it was checked that the thresholds of the longitudinal coupled bunch instabilities of modes trapped around the resulting open gap are above the maximal applied beam current of 400 mA.

INTRODUCTION

The 4 injection kickers in the ALBA storage ring are out of vacuum magnets. The yoke is C shape made with 22 mm thick ferrite plates. The one turn conductor is only running on the inner side while a copper plate used as eddy current shield is installed at the outer side. The ceramic chambers have a race track cross section with an aperture H x V= 80 x 24 mm and a length of 680 mm and have provisions to be air cooled. The thickness of the ceramic is 5 mm (Fig. 1). The

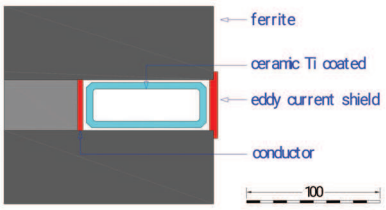

Figure 1: Cross section of Storage Ring injection kicker.

chamber was coated with a nominal 400 nm thick Ti-layer (overall resistance 4.3 Ω) by a magneton sputter source. For a homogeneous Ti-layer over the whole range the coating was deposited in several strokes. First test on a glass sample was performed in order to determine the electrical resistance to thickness ratio, as after deposition on a ceramic chamber the thickness cannot be easily measured. Then, when the first chamber was coated, it turned out that the measured overall resistance was by a factor of 5 larger to what had been expected from a nominal 400 nm thick Ti layer. This is due to the contribution of the surface roughness of the ceramic with grain sizes about 5–10 μm which increases the effective resistance of the coating. The chambers were finally coated to achieve a nominal resistance of 4.3 Ω and no thickness measurement was performed afterwards. The ceramic pipe had an inner diameter of 24 mm to which the manufacturer planned to braze a metallic pipe with an inner diameter of 29 mm. Due to production reasons, mainly risking the cracking of the ceramic the manufacturer did not want reduce the diameter of the metallic tube. The proposed solution was

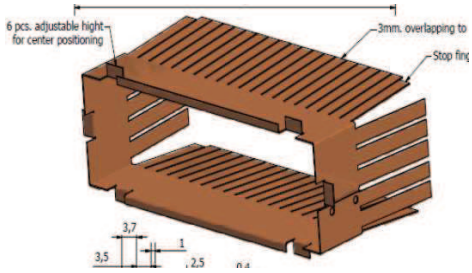

Figure 2: RF-finger.

Figure 3: Collapsed RF-finger .

to add an inner RF-finger to meet both surfaces. The RF-finger is 0.25 mm thick and made of BeCu. A picture of the manufactured RF-fingers is shown in Fig. 2. A spare chamber with two pinger magnets installed around it was used later on [1], so we ended up having 5 ceramic chambers with 2 RF-fingers each in the storage ring installed.

ISSUES

Already from the start there was the doubt whether the electrical contact between the RF-finger and the metallic layer on the ceramic would be good enough during operation. Therefore thermocouples were placed at the entry and exit of each ceramic, on the metallic pipe to continuously monitor the temperature at the RF-fingers and be able to detect any unexpected change of behaviour. Indeed, during commissioning of the storage ring and while the current in the machine was being increased, the upper part of the RF-finger at the entry of KI03 collapsed towards the center of the vacuum pipe, making injection not possible and therefore requiring immediate exchange (see Fig. 3). This type

* tguenzel@cells.es

ISBN: 978-3-95450-184-7 doi:10.18429/JACoW-IPAC2018-TUPMK001

of accident happened once more following a machine day. The RF-finger at the exit of the pinger collapsed in exactly the same way. In addition to these two accidents in the last 7 years, the thermocouples placed in the ceramic chambers have always shown the largest dependence on current in the machine, being it multibunch or single bunch. Figure 4 compares temperatures around the pinger magnet with and without the RF-fingers in place. The temperatures decrease by up to 8° C, sometimes even up to 10° C.

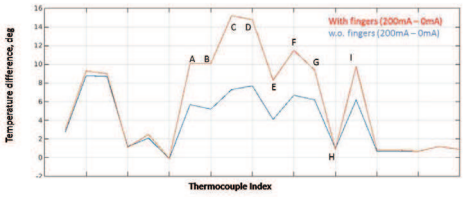

Figure 4: Temperature decrease in the pinger after the RF-finger removal.

SIMULATIONS

The observed behaviour of the ceramic chambers are backed up by impedance (T(-domain)) & eigenmode (F(-domain)) GdfidL-simulations [2]. In the following the kicker and pinger will be distinguished. In difference to the pinger, the kicker has slightly different outlet pipe cross sections and on top of it the beam circulates 4mm off-centered which changes the shunt impedance of a mode. The analysis will be limited by the cut-off frequency as modes above the cut-off are considered to escape easily the geometry and therefore are not potentially dangerous.

Transverse Impedance

Due to the rather large cavities created by the chambers next to the ceramic tube left without RF-fingers the increase of the vert. transverse impedance is quite important. For the calculation of the transverse impedance only the dipolar part of the total wake was considered. The β-weighted dipolar impedance increases by a factor 4 (Table 1).

Table 1: β_V-Weighted Eff. Vertical Impedance (in kΩ)

element	β_V [m]	with RF-fingers	w/o RF-fingers
kicker	7.5	3.15	11.9
pinger	5.2	2.18	9.4

Longitudinal Spectra

The longitudinal impedance spectra analysis was combined with the one of the eigenmodes computed by GdfidL. T- and F-domain computations are actually not equivalent but both provide a complementary image of the full picture. The resonances, in particular their frequencies, found in the impedance spectra are rather precise, and show a rather complete picture in terms of modes whereas the eigenmode computations depend on a couple of external parameters difficult to optimise. On top of it the eigenmode solver generates much more modes than resonances exist, so some of them are just propagating (not real). But they provide a shunt impedance R_s whereas the height of resonances in impedance spectra depend on the length of the trailer of the witness particle. The shunt impedance, however, can be directly compared to the threshold of longitudinal coupled bunch instabilities (LCBI). The shunt impedance value here is only based on the dissipative quality factor which does not consider losses and its corresponding quality factor (called radiative losses) generated by a slipping of the resonance' field out of its trapping location. In general the dissipative shunt impedance is sufficient as adding further losses will only reduce it more[1]. Both data are shown in an overlay of the eigenmode's shunt impedance on the real's part impedance spectrum in logarithmic scale in order to cover a large dynamic range.

The Threshold Criterion

It essentially requires the sampling of the impedance $Z_l(\omega_m)$ (ω_m is assumed to hit the peak once, with low Q multiple hits on the peak are possible, then R_s will be small) at the resonance peak $\omega_m = (Mj\omega_0 + m\omega_0)$ and at $-(Mj\omega_0 - m\omega_0)$) close to the mirror peak $Z_l(-\omega_m)$ (ω_0 as angular rev. frequency, M the harmonic number and j any integer, $m = 1, \ldots, M$) of which the negative contribution can partially cancel out the positive one. Neglecting in the following the negative contribution altogether makes the criterion stricter, but much simpler. As long as resonances stay below the threshold of this criterion LCBIs cannot be excited. The suchlike sampled impedance is compared to (I_1 being the 1. modified bessel function):

$$R_s^{threshold} = \frac{\omega_s \omega_r \sigma_\tau^2 T_0 (E/e)}{\tau I \alpha \exp(-(\omega_r \sigma_\tau)^2) I_1((\omega_r \sigma_\tau)^2)}$$

where ω_s and ω_r stand resp. for the angular synchrotron and resonance frequency, σ_τ for bunch length, $T_0 = 2\pi/\omega_0$, τ for long. damping time and E for the beam energy, α for the momentum compaction factor and I the multibunch current, here 0.4A. Normally the assumption $I_1(x) \approx 0.5x$ for $x \ll 1$ is made which is no longer true for $\omega_r/(2\pi) \approx 5 - 7$GHz.

Longitudinal Loss Factors

Table 2 shows the incoherent loss factors found from the impedance (T) and eigenmode spectra (F). In case of 400 mA homogeneous filling the loss factors have to be multiplied by a factor 0.32 in order to obtain the power loss @0.4 A. However, most of the losses above cut-off will propagate out of the structure and therefore do not contribute to its heat-load. The eigenmode spectra were studied upon possible coincidences with the bunch repetition frequency which can lead to coherent loss. A coincidence @6.49 GHz was found. But the corresponding impedance spectrum resonance – considered as more precise – was slightly shifted with respect

[1] In the meantime GdfidL provides a combination of both, but disposing of both distinguished information was preferred.

ISBN: 978-3-95450-184-7 doi:10.18429/JACoW-IPAC2018-TUPMK001

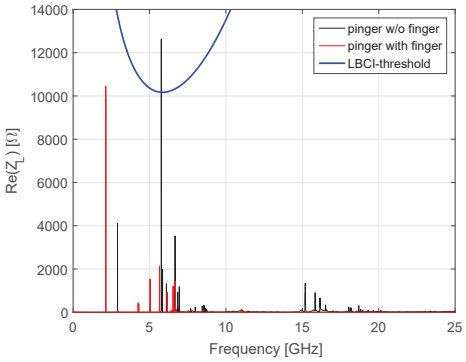

Figure 5: Pinger impedance with and without fingers.

Table 2: Loss Factor ($\frac{mV}{pC}$)(σ_τ=20.8 ps), Cutoff ~ 6.8 GHz

element	kicker		pinger	
domain	T	F	T	F
with finger(<cutoff)	86.4	83.18	88.3	70.8
w/o finger (<cutoff)	47.5	32.54	59.2	54.5
with finger(no cutoff)	91.8		92.9	
w/o finger (no cutoff)	123.0		147.3	

to the eigenmode frequency. So this coincidence was not taken for real.

ANALYSIS

Figure 5 shows very well the situation. The finger protect the chambers from high resonances around 6 GHz, the reason for their initial installation. With fingers the losses below the cut-off distribute over a larger number of resonances which makes it larger than without fingers where it is more concentrated on only a few resonances. Above cut-off it is different: the losses with fingers are rather small whereas without fingers they are large. Without fingers the apparent high resonances can be actually afforded (those of Fig. 5 too) by accounting for both types of losses – the dissipative (F) and the radiative (expressed in the width and height of the peaks) losses (T) – so their height will stay below the threshold criterion. Actually, considering only dissipative losses is already sufficient. The Fig. 6, 7, 8 and 9 show that all R_s-values stay below the threshold curve (the combination of both loss types, however, is not shown graphically). There is also good agreement between the impedance and the eigenmode spectra. The main benefit of the removal of the RF-fingers is the decrease of the losses below the cut-off which directly reduces the heatload whereas above the cut-off it is bearly affected by the losses.

CONCLUSION

After removing half of the RF-fingers installed in the SR ring, we do not seem to suffer anymore from unexpected temperature increases at the ceramic chambers which lead to the damage of the fingers. Therefore, we plan to stay like this in the future and do not pursue the removal of additional fingers. The higher transverse impedance was put up with.

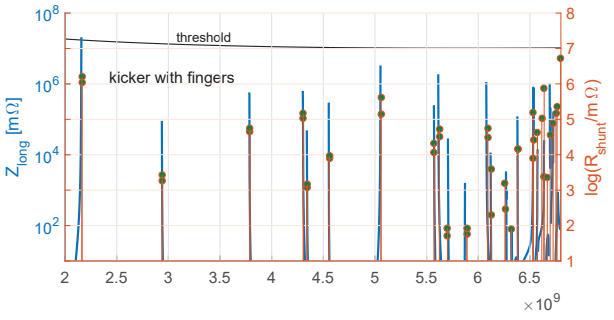

Figure 6: $Re(Z_l)$(blue) & R_s of the eigenmodes (orange).

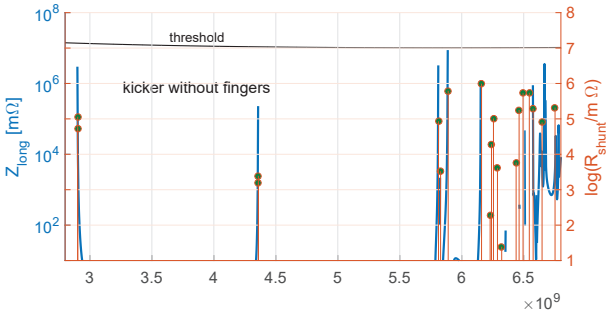

Figure 7: $Re(Z_l)$(blue) & R_s of the eigenmodes (orange).

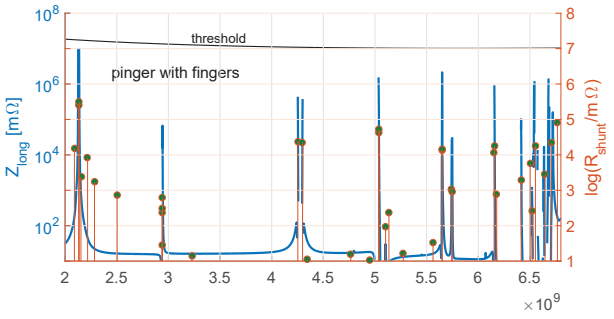

Figure 8: $Re(Z_l)$(blue) & R_s of the eigenmodes (orange).

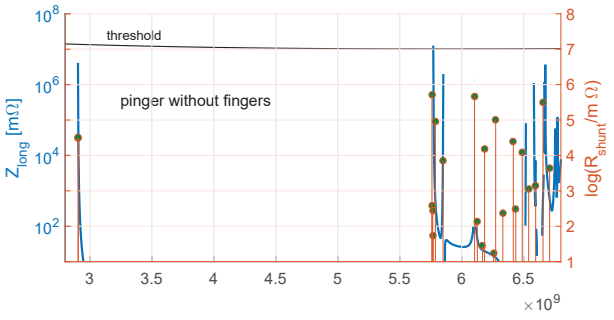

Figure 9: $Re(Z_l)$(blue) & R_s of the eigenmodes (orange).

REFERENCES

[1] M.Pont et al. "A pinger magnet system for the ALBA Synchrotron light Source", in Proc. IPAC'2015, pp. 3039-3042

[2] W. Bruns, http://www.gdfidl.de